Force Generated by Two Kinesin Motors Depends on the Load Direction and Intermolecular Coupling

Hamid Khataee and Jonathon Howard*
Department of Molecular Biophysics and Biochemistry, Yale University, New Haven, Connecticut 06511, USA

(Received 10 August 2018; revised manuscript received 16 December 2018; published 8 May 2019)

Kinesins are molecular motors that carry cellular cargoes. While the mechanics of single kinesins are well characterized experimentally, the behavior of multiple kinesins varies considerably among experiments. The basis for this variability is unknown. Here, we resolve single-motor force measurements into a vertical component, which accelerates kinesin detachment, and a horizontal component, which decelerates the detachment when resisting the motor. This directionality, when the different experimental geometries are considered, can account for much of the variation in multiple motor dynamics.

DOI: 10.1103/PhysRevLett.122.188101

Introduction.—The dimensions of eukaryotic cells, greater than 10 μm in diameter, are such that diffusion is an inefficient mechanism for intracellular transport. To augment diffusion, molecular motors transport cellular cargoes in a directed manner along intracellular filaments using adenosine triphosphate (ATP) as the chemical fuel. An example is kinesin-1, which transports cargo away from the cell center in neurons and other cells [1]. Single kinesin molecules are processive, meaning that they are able to take hundreds of steps along a microtubule (MT) before detaching [2–4], ensuring that cellular cargoes are transported reliably over long distances. *In vitro* assays, in which the activity of purified proteins are reconstituted in cell free environments, in combination with optical tweezers and sensitive fluorescence microscopy techniques, have provided a detailed picture of how the processivity and the velocity of kinesin depends on external force, as well as the ATP concentration [5,6]. Thus, kinesin is a very well characterized molecular motor, at least when it is operating individually.

Though single kinesin molecules are capable of moving cargoes in cells [7], there are many cases in which intracellular transport is driven by ensembles of motors. For example, multiple kinesins are involved in mitotic spindle assembly during cell division [8], drive transport trains in cilia [9], and transport oil droplets in developing flies [7]. In contrast to the single-molecule studies, measurements of the mechanical properties of ensembles of kinesins have yielded highly variable results (Table I). For example, gliding assays in which motors attached to a planar surface slide microtubules across the surface, clearly show that multiple kinesins can generate as much as 10 times the single-molecule force [10] (and see also Refs. [11–13]). By contrast, bead assays in which motors attached to a glass bead walk along a fixed microtubule, show that two to four motors generate no more force than a single molecule [14,15]. These differences presumably arise from differences in the experimental conditions, but it is not known which variations are critical.

Earlier theoretical studies have modeled cargo transport by multiple motors [21–25] but have not been able to predict the experimentally observed velocities and run times (average time to detachment) at high forces [17]. These models all assumed a symmetric force-detachment rate relation for a single kinesin; i.e., the detachment rate under assisting forces (applied in the stepping direction, positive) is equal to that under resisting or loading forces (applied against the stepping direction, negative). However, recent force measurements of Block and colleagues [26] have provided clear evidence that the detachment rate under assisting forces is greater than that under resisting forces. In this Letter, we develop a theoretical framework that provides a novel interpretation for this asymmetry. This interpretation, when applied to multiple motor assays, predicts that different experimental geometries give rise to different load-dependent detachment rates. As a consequence, variations in the vertical direction of the applied forces, due to different lengths of motor constructs and sizes of beads, together with the strength of coupling between motors, can account for the broad range of experimental findings.

Single-kinesin detachment rate.—Block and colleagues [26] recently discovered that the force-detachment rate for single kinesin molecules is asymmetric; see Fig. 1(a). We interpret this asymmetry as follows. The optical forces ($\boldsymbol{F}$) acting on the beads and transferred to the motors have both vertical (F_z) and horizontal (F_x) components, which act through the center of the bead and have similar magnitudes, due to the geometry; see Fig. 1(a), inset. We propose that because both assisting and resisting forces increase the detachment rate, the vertical force component must be dominant and accelerates detachment [Fig. 1(b), green curve]. However, the detachment rate is much steeper

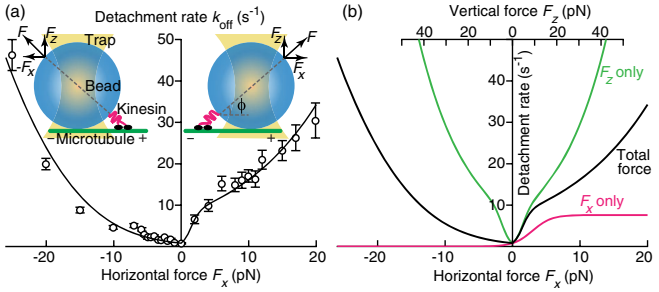

FIG. 1. Force-detachment rate for single kinesin-1. (a) The detachment rate vs the horizontal force component applied by the optical trap [open circles: experimental data (mean ± SE) at 2 mM ATP [26]]. The continuous curve is our two-step detachment model in Eq. (1); and see Fig. S1, Supplemental Material [31]. Inset: the plastic bead (blue) with kinesin attached by its tail (magenta) with its heads (black) moving rightwards along the microtubule (green). The drawing is approximately to scale. For a 440-nm-diameter bead and a 35-nm-long kinesin used in the experiments [26], the angle between kinesin and MT is $\phi = 60°$. The vertical force component F_z is the same irrespective of the sign of the horizontal force component F_x, i.e., assisting (to the right, positive) or resisting (to the left, negative). (b) Decomposition of the force-detachment dependence into horizontal and vertical force dependencies. The black curve is the output of our model in (a) where the motor is subject to both horizontal and vertical forces. The green (magenta) curve is the detachment rate in the presence of only vertical (horizontal) force.

for small assisting forces; we therefore propose that the horizontal component accelerates detachment when it is assisting, but slows detachment when it is resisting [Fig. 1(b), magenta curve]. Thus, for vertical forces kinesin exhibits slip-bond behavior; i.e., the detachment rate increases with force [27]. But, for horizontal forces, kinesin exhibits catch-bond behavior; i.e., the detachment rate decreases with resisting (load) force, and increases for assisting forces. The presence of the catch bonding is surprising, because previous studies assumed that catch bonding is absent in kinesin and kinesin has slip-bond behavior only [28–30]. Importantly, catch-bond behavior is expected to dominate when the forces are parallel to the MT [Fig. 1(b), magenta curve].

To account for the data quantitatively, especially with the inflection on the right-hand side of the curve [Fig. 1(a), ~3 pN], we introduce a second idea: the detachment of kinesin from the MT is a two-step process. Accordingly, kinesin detachment passes through three states: strongly bound state $\xrightarrow{k_1}$ weakly bound state $\xrightarrow{k_2}$ detached state, with effective off rate,

$$k_{\text{off}} = k_1 k_2/(k_1 + k_2), \tag{1}$$

Both rates k_1 and k_2 depend on the horizontal and vertical force components described in the previous paragraph, and the inflection corresponds to the changeover from k_1 being rate limiting to k_2 being rate limiting. The force dependence is modeled using transition states that are displacement vectors with both vertical and horizontal components, following Refs. [32,33] who modeled measurements of the load-dependence of kinesin velocity (Refs. [34,35]). Accordingly, $k_j = k_j^0 e^{(\boldsymbol{F}\cdot\boldsymbol{\delta}_j)/k_B T}$, where k_j^0 (for $j = 1, 2$) are the unloaded rates, $\boldsymbol{F} = (F_x, F_z)$ and $\boldsymbol{\delta_j} = (\delta_{x_j}, \delta_{z_j})$ denote the force and displacement vectors, respectively, and $k_B T$ is the thermal energy. This novel interpretation of the force-detachment rate relation allows us to model the experimental data accurately by the continuous curve [Fig. 1(a)] with five free parameters: $k_1^0 = 0.91 \pm 0.38\ \text{s}^{-1}$, $\delta_{x_1} = 2.90 \pm 1.24$ nm, $\delta_{z_1} = 2.25 \pm 0.75$ nm, $k_2^0 = 7.62 \pm 0.74\ \text{s}^{-1}$, and $\delta_{z_2} = 0.18 \pm 0.01$ nm (mean ± SE). δ_{x_2} was set to zero as a nonzero value gave no further improvement to the fit. Thus, the two-step detachment model in which the steps depend on vertical and horizontal components provides a quantitative description of the detachment-rate data. Note that if the strong-to-weak transition was rapidly reversible with equilibrium constant $K(\boldsymbol{F})$, then analogous equations would be obtained with $k_1' = Kk_2$.

Equation (1) with force-dependent rates allows us to predict detachment rates and run lengths under different geometries (Fig. 2), such as beads of different sizes or when the forces are directly applied along the MT axis in gliding assays. Note that the run-length calculations require information about the force dependence of the single-motor velocity v_{si} which, for simplicity, we assume only depends on the horizontal forces (see Ref. [31] for details, but see Refs. [32,33]). The model predicts that the run times ($1/k_{\text{off}}$) and distances will be maximum when parallel forces resist the motor (Fig. 2); such long run times and distances at high forces were observed in gliding assays where the forces are primarily parallel [13]. Also, it predicts that if the kinesin tether is shorter or the bead radius is larger, the larger angle ϕ between kinesin and MTs will lead to a larger vertical force and the run times and lengths will decrease (i.e., less processivity), as observed in Refs. [14,36].

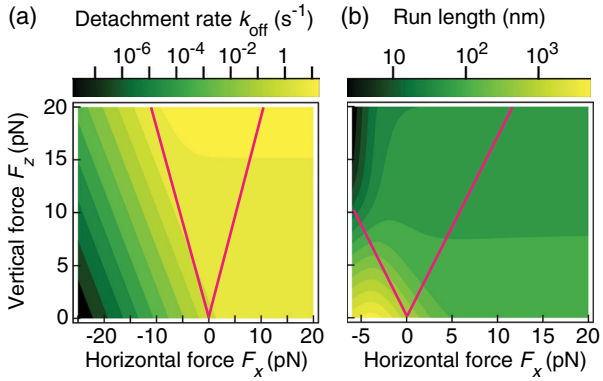

FIG. 2. Detachment rate and run length of single kinesin vs vertical and parallel force components. Lines (magenta) correspond to the force direction in experiments [26]. (a) Detachment rate is calculated using Eq. (1). (b) Mean run length is calculated as $v_{\text{si}}/k_{\text{off}}$, where v_{si} is the single-kinesin velocity (see Ref. [31]).

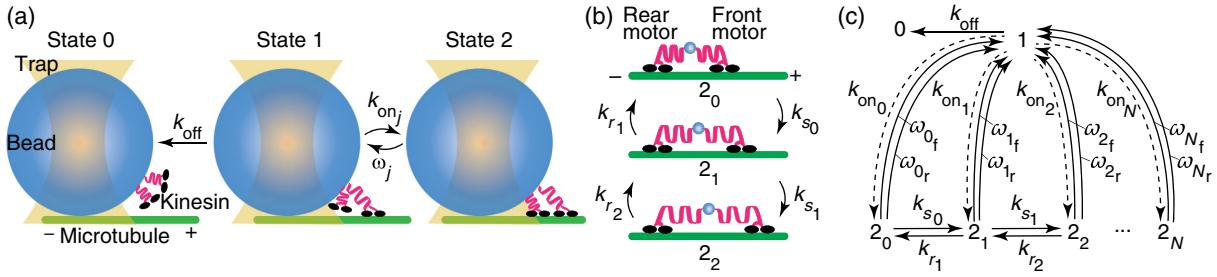

FIG. 3. Model of the two-kinesin complex. (a) States with zero (left), one (middle), and two (right) motors bound to a microtubule. (b) Representations of state 2 in which the vertical forces have been set to zero for clarity. The force acts at the bead (blue). Top: the strain in the spring (magenta) connecting the motors (black) is zero. Middle: the strain is $d/2$ as the front motor takes a step to the right. Bottom: the strain is d as the front motor takes another step forward. (c) Kinetic scheme for the two-motor complex. The states 0, 1, and 2 correspond to those in (a). The states 2_j correspond to those in (b) with $j = 0, 1, 2, \ldots, N$. k_{s_j} (k_{r_j}) denotes the stretching (relaxation) rate of the complex. ω_{j_f} (ω_{j_r}) denotes the detachment rates of the front (rear) motor. k_{on_j} is the attachment rate of a motor to a site with strain $jd/2$.

Two-motor model.—Having modeled the dynamics of a single kinesin, we asked how the collective mechanics of multiple kinesins depends on the force direction. We have restricted our analysis to just two kinesins for simplicity, and because when more than two motors move a cargo it is difficult to count the number [15,37], though this problem has been solved using DNA origami [14]. We propose a three-state model: cargo detached (state 0), attached by one motor (state 1), and attached by two motors (state 2); see Fig. 3(a). We assume that every run of the complex starts in state 1, and the motors step forward asynchronously.

To model intermolecular forces, we couple kinesins to a cargo via their tails, which act as linear springs with stiffness κ, a measure of the strength of coupling between the motors. Each motor in the complex is subjected to forces, which can arise externally or internally. External applied force F_{app} is shared equally by the two motors, whereas internal forces increase with the strain between the motors. In the equilibrium configuration 2_0, where the motors are relaxed, internal forces are zero. When one motor steps through a distance d, it displaces cargo by $d/2$ [37] and the internal force of magnitude $\kappa d/2$ is exerted onto each motor in the opposite directions [Fig. 3(b)]. Accordingly, discrete stepping of motors partitions state 2 into substate configurations 2_j in which intermolecular forces of magnitude $\kappa jd/2$ are exerted onto each motor in the opposite directions, where $j = 0, 1, 2, \ldots, N$ denotes the absolute value of the strain between the two motors (in units of $d/2$). For computational reasons, using the method proposed in Ref. [38] and used in Refs. [22,39,40], N is truncated when the occupancy probability of the most strained state falls below 1%, with a minimal effect on the calculations; see Fig. 3(b) and Ref. [31] for details. Thus, in every configuration 2_j, the total force applied on the front motor is $F_f = (F_{\mathrm{app}} - \kappa jd)/2$ and on the rear motor is $F_r = (F_{\mathrm{app}} + \kappa jd)/2$. We next calculate the rates at which the complex is stretched and relaxed. Stepping of the front (rear) motor stretches (relaxes) the complex, causing the transition from state 2_j to state 2_{j+1} (from state 2_j to state 2_{j-1}). Thus, the stretching and relaxation rates are defined by the stepping rates of the front and rear motors as $k_{s_j} = v_{\mathrm{si}}(F_f)/d$ and $k_{r_j} = v_{\mathrm{si}}(F_r)/d$, respectively.

The forces applied to the motors also influence the rates that one of the motors may detach and reattach to the MT. Transition from a two-motor configuration 2_j to the one-motor state 1 occurs with the detachment of the either of motors with rates $\omega_j = k_{\mathrm{off}}(F_f) + k_{\mathrm{off}}(F_r) = \omega_{j_f} + \omega_{j_r}$; see Fig. 3(c). On the other hand, the transition rate from state 1 to a two-motor configuration 2_j depends inversely on the strain energy of the complex in that configuration. We define the attachment rate to a configuration 2_j as $k_{\mathrm{on}_j} = k_{\mathrm{on}_0} e^{-E_j/k_B T}$, where k_{on_0} is the transition rate into the relaxed state 2_0 and E_j is the strain energy of the complex in state 2_j; see Fig. 3(c). To calculate k_{on_0}, we use the experimentally estimated ensemble attachment rate $\mathcal{K}_{\mathrm{on}} = 5\ \mathrm{s}^{-1}$ [12]. Since $\mathcal{K}_{\mathrm{on}} = \sum_{j=0}^{N} k_{\mathrm{on}_j}$, one can calculate $k_{\mathrm{on}_0} = \mathcal{K}_{\mathrm{on}} / \sum_{j=0}^{N} e^{-E_j/k_B T}$. The strain energy is $E_j = (1/2)\kappa_{\mathrm{complex}}(jd)^2 = (1/4)\kappa(jd)^2$, where $\kappa_{\mathrm{complex}} = (1/2)\kappa$ is the effective coupling strength.

Having all transition rates in the kinetic scheme in Fig. 3(c), we calculate the mean run time, run length, and velocity of the two-motor complex. First, we calculate the probability of finding the cargo in every state of the scheme by defining the following set of master equations:

$$
\begin{aligned}
&\partial_t P_0(t) = k_{\mathrm{off}} P_1(t),\\
&\partial_t P_1(t) = -\left(\sum_{j=0}^{N} k_{\mathrm{on}_j} + k_{\mathrm{off}}\right) P_1(t) + \sum_{j=0}^{N} \omega_j P_{2_j}(t),\\
&\partial_t P_{2_0}(t) = k_{\mathrm{on}_0} P_1(t) - (\omega_0 + k_{s_0}) P_{2_0}(t) + k_{r_1} P_{2_1}(t),\\
&\partial_t P_{2_j}(t) = k_{\mathrm{on}_j} P_1(t) + k_{s_{j-1}} P_{2_{j-1}}(t)\\
&\qquad\qquad - (\omega_j + k_{s_j} + k_{r_j}) P_{2_j}(t) + k_{r_{j+1}} P_{2_{j+1}}(t), \quad 1 \le j < N,\\
&\partial_t P_{2_N}(t) = k_{\mathrm{on}_N} P_1(t) + k_{s_{N-1}} P_{2_{N-1}}(t) - (\omega_N + k_{r_N}) P_{2_N}(t),
\end{aligned}
\tag{2}
$$

where $P_0(t)$, $P_1(t)$, and $P_2(t) = \sum_{j=0}^{N} P_{2_j}(t)$ denote the probabilities of finding the cargo in states 0, 1, and 2 at time t (Fig. S3 in the Supplemental Material [31]). We numerically solve Eq. (2) (see Ref. [31] for details) and define the complex's mean run time $\langle t \rangle = \int_0^\infty t[\partial_t P_0(t)]dt$, mean run length $\langle l \rangle = \lim_{t\to\infty} \int_0^t \tilde{v} dt$, where the ensemble velocity is $\tilde{v} = v_{si} P_1(t) + \sum_{j=0}^{N}(\{[(v_{si}(F_f) + v_{si}(F_r)/2]P_{2_j}(t)\} + (jd/2)(\omega_{j_f} - \omega_{j_r}))$, and velocity $v = \langle l \rangle / \langle t \rangle$.

Two-motor dynamics.—Our model accounts for much of the variation of collective properties of kinesins in different multimotor assays. For bead assays, it predicts that two weakly coupled kinesins ($\kappa = 0.05$ pN/nm) have greater run times and run lengths than a single kinesin; see Figs. S4(a)–S4(b) [31]. At low forces, when the coupling stiffness is expected to be low due to segmental flexibility [20], the run times and lengths are predicted to be 2 times larger than those for single motors; this is because the weak coupling results in small vertical forces and so the detachment rate is low and the probability that transport is mediated by two MT-bound motors is high (Fig. S3 [31]), leading to higher processivity. This accords with the high processivity observed at zero force: adding a second motor approximately doubles the run time [17,18] and the run length [14,17–19]; see Table I and Figs. 4(a)–4(b). Thus, our model accounts for the dependence of processivity on motor number.

Our model further predicts that at zero force the two-motor velocity is almost independent of the coupling strength and is close to the single-motor velocity [Fig. 4(c) and Fig. S4(c) in the Supplemental Material [31]]. This agrees with experiments that single-, two-, and many-kinesin velocities are similar at zero forces (Table I). Our model can also account for a curious observation made in Refs. [15,17] that the velocity increases with resisting force (at a high force): in Fig. S4(c) [31] there is a crossover of the force-velocity curves as the coupling increases (at ~ -7 pN) so an increase in velocity could be due to a strong force-dependent increase in coupling.

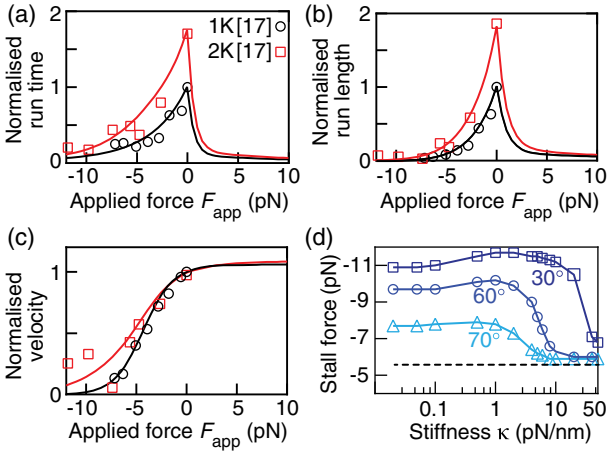

FIG. 4. Force run time, force run length, force velocity, and stall force. (a)–(c) Simulations of bead assays ($\phi = 60°$) are for single kinesin (black curve) and for two kinesins with coupling stiffness $\kappa = 0.4$ pN/nm (red curve). One- and two-kinesin (1K and 2K) experimental data are from Ref. [17]. Run time, run length, and velocity are normalized to their corresponding values for single kinesin at zero force. (d) Stall force for single and two kinesins vs κ at different angles ϕ. The dashed line is the single-kinesin stall force (~ -5.5 pN for all angles).

Thus, the model accords with the observed collective velocities.

Finally, and importantly, our model can account for the broad range of forces measured in the different assays. When the vertical forces are small (e.g., gliding assays or small beads and full-length motors) and the coupling stiffness is < 1 pN/nm, we find that the two-kinesin stall force (where velocity falls to 10% of the unloaded velocity) is almost twice that for a single kinesin [Fig. 4(d)]. This prediction accords with gilding assays: multiple motors can slide microtubules for 300 nm against forces as high as 100 pN [10] (and also see Refs. [11,13]), which is much larger than the single-motor force in gliding assays [11]. This high force further supports the notion that kinesin has

TABLE I. Variation of the properties of kinesin motors found in different assays.

Parameter	One motor	Two motors			Many motors		
Maximum force[m]	f	$\sim f$ [14][d][15][e]	$\sim 2f$ [7][g][16][f]	$\gg f$ ...	$\sim f$ [14][d]	$\sim 2f$ ...	$\gg f$ [10][a][11][a][12][b][13][a]
Run length (at zero force)	L	$\sim L$ [7][g]	$\sim 2L$ [14][d][17][e][18][h][19][e]	$\gg L$ [16][f]	$\sim L$ ...	$\sim 2L$ ...	$\gg L$ [2][a][3][c][14][d][16][f][18][h]
Velocity (at zero force)	v	$\sim v$ [7][g][14][d][18][h]	$\sim 2v$ ...	$\gg v$ ...	$\sim v$ [2][a][3][c][14][d][18][h]	$\sim 2v$ ...	$\gg v$ ...

[a,b]MT gliding assay. Bead assays with different bead diameters: [c]200 nm and [d,e,f]450–500 nm. [g]650-nm diameter oil droplet *in vivo*. [h]Assays with fluorescently labeled motors coupled to DNA scaffolds. Kinesins with different contour lengths: [a,c,f,g]full length (~50 nm), [e,h]truncated at ~aa560 (~35 nm), [b,d]truncated at ~aa430 (~17 nm). The angles ϕ between kinesins and MT: [d]~68 – 70°, [e,g]~60–62°, [f]~55-56°, [c]~42°, and [a,b,h]~30°. The last angle is assumed for gliding assays. The length is shorter under zero force due to entropic folding [20]. In Refs. [14,18] and [15,17] the motor number is precisely controlled using DNA and protein scaffolds, respectively. Except for Ref. [10], all other assays have corresponding single-motor measurements. [m]Maximum force is the average peak force.

catch-bond behavior for parallel forces [Fig. 1(b)]. This prediction also accords with bead experiments where two motors have stall forces approximately twice the single-molecule stall force (Refs. [7,16], Table I). However, when the vertical forces are high, we find that the stall force of two motors can be similar to that of a single motor [Fig. 4(d), coupling stiffness is > 5 pN/nm]. The reason is that the detachment rate is high [Fig. 2(a)]. This accords with bead force measurements in Ref. [14] with a short motor construct ($\phi \sim 70°$) in which the maximum force, defined as the average peak force (when motors detach), was similar for two (or more) motors as it was for one motor. Thus, we conclude that variations in the force direction and in the coupling strength between motors can account for a broad range of experimental findings.

We thank Sujoy Ganguli for his constructive feedback on an early version of the results. We are grateful to Karla Neugebauer, Sabyasachi Sutradhar, Mohammed Mahamdeh, and Dietmar Oelz for critical comments on the manuscript. This work was funded by National Institutes of Health DP1 MH110065 to J. H.

*Corresponding author.
jonathon.howard@yale.edu

[1] J. Howard, *Mechanics of Motor Proteins and the Cytoskeleton* (Sinauer, Sunderland, MA, USA, 2001).
[2] J. Howard, A. J. Hudspeth, and R. D. Vale, Nature (London) **342**, 154 (1989).
[3] S. M. Block, L. S. B. Goldsteint, and B. J. Schnapp, Nature (London) **348**, 348 (1990).
[4] R. D. Vale, T. Funatsu, D. W. Pierce, L. Romberg, Y. Harada, and T. Yanagida, Nature (London) **380**, 451 (1996).
[5] N. J. Carter and R. A. Cross, Nature (London) **435**, 308 (2005).
[6] M. J. Schnitzer, K. Visscher, and S. M. Block, Nat. Cell Biol. **2**, 718 (2000).
[7] G. T. Shubeita, S. L. Tran, J. Xu, M. Vershinin, S. Cermelli, S. L. Cotton, M. A. Welte, and S. P. Gross, Cell **135**, 1098 (2008).
[8] D. J. Sharp, G. C. Rogers, and J. M. Scholey, Nature (London) **407**, 41 (2000).
[9] L. Stepanek and G. Pigino, Science **352**, 721 (2016).
[10] V. Bormuth, A. Jannasch, M. Ander, C. M. Van Kats, A. Van Blaaderen, J. Howard, and E. Schäffer, Opt. Express **16**, 13831 (2008).
[11] A. J. Hunt, F. Gittes, and J. Howard, Biophys. J. **67**, 766 (1994).
[12] C. Leduc, O. Campas, K. B. Zeldovich, A. Roux, P. Jolimaitre, L. Bourel-Bonnet, B. Goud, J.-F. Joanny, P. Bassereau, and J. Prost, Proc. Natl. Acad. Sci. U.S.A. **101**, 17096 (2004).
[13] E. Meyhöfer and J. Howard, Proc. Natl. Acad. Sci. U.S.A. **92**, 574 (1995).
[14] K. Furuta, A. Furuta, Y. Y. Toyoshima, M. Amino, K. Oiwa, and H. Kojima, Proc. Natl. Acad. Sci. U.S.A. **110**, 501 (2013).
[15] D. K. Jamison, J. W. Driver, A. R. Rogers, P. E. Constantinou, and M. R. Diehl, Biophys. J. **99**, 2967 (2010).
[16] M. Vershinin, B. C. Carter, D. S. Razafsky, S. J. King, and S. P. Gross, Proc. Natl. Acad. Sci. U.S.A. **104**, 87 (2007).
[17] D. K. Jamison, J. W. Driver, and M. R. Diehl, J. Biol. Chem. **287**, 3357 (2012).
[18] N. D. Derr, B. S. Goodman, R. Jungmann, A. E. Leschziner, W. M. Shih, and S. L. Reck-Peterson, Science **338**, 662 (2012).
[19] J. Xu, Z. Shu, S. J. King, and S. P. Gross, Traffic **13**, 1198 (2012).
[20] J. Kerssemakers, J. Howard, H. Hess, and S. Diez, Proc. Natl. Acad. Sci. U.S.A. **103**, 15812 (2006).
[21] F. Berger, C. Keller, S. Klumpp, and R. Lipowsky, Phys. Rev. Lett. **108**, 208101 (2012).
[22] F. Berger, C. Keller, S. Klumpp, and R. Lipowsky, Phys. Rev. E **91**, 022701 (2015).
[23] S. Klumpp and R. Lipowsky, Proc. Natl. Acad. Sci. U.S.A. **102**, 17284 (2005).
[24] A. Kunwar, M. Vershinin, J. Xu, and S. P. Gross, Curr. Biol. **18**, 1173 (2008).
[25] W. Nam and B. I. Epureanu, PLoS Comput. Biol. **11**, e1003981 (2015).
[26] J. O. L. Andreasson, B. Milic, G. Y. Chen, N. R. Guydosh, W. O. Hancock, and S. M. Block, eLife **4**, e07403 (2015).
[27] M. Dembo, Proc. R. Soc. London, Ser. B **234**, 55 (1988).
[28] A. Nair, S. Chandel, M. K. Mitra, S. Muhuri, and A. Chaudhuri, Phys. Rev. E **94**, 032403 (2016).
[29] A. Yamada, A. Mamane, J. Lee-Tin-Wah, A. Di Cicco, C. Prévost, D. Lévy, J. F. Joanny, E. Coudrier, and P. Bassereau, Nat. Commun. **5**, 3624 (2014).
[30] C. Leduc, N. Pavin, F. Jülicher, and S. Diez, Phys. Rev. Lett. **105**, 128103 (2010).
[31] See Supplemental Material at http://link.aps.org/supplemental/10.1103/PhysRevLett.122.188101 for decomposition of detachment steps, single-kinesin velocity, solving master Eq. (2), probability distribution over states 0, 1, and 2, and two-kinesin dynamics versus coupling stiffnesses.
[32] M. E. Fisher and Y. C. Kim, Proc. Natl. Acad. Sci. U.S.A. **102**, 16209 (2005).
[33] M. E. Fisher and A. B. Kolomeisky, Proc. Natl. Acad. Sci. U.S.A. **96**, 6597 (1999).
[34] S. M. Block, C. L. Asbury, J. W. Shaevitz, and M. J. Lang, Proc. Natl. Acad. Sci. U.S.A. **100**, 2351 (2003).
[35] F. Gittes, E. Meyhöfer, S. Baek, and J. Howard, Biophys. J. **70**, 418 (1996).
[36] K. Svoboda and S. M. Block, Cell **77**, 773 (1994).
[37] C. Leduc, F. Ruhnow, J. Howard, and S. Diez, Proc. Natl. Acad. Sci. U.S.A. **104**, 10847 (2007).
[38] T. L. Hill, Proc. Natl. Acad. Sci. U.S.A. **85**, 2879 (1988).
[39] H. Khataee and A. W. C. Liew, Bioinformatics **30**, 353 (2014).
[40] H. Khataee, S. Naseri, Y. Zhong, and A. W. C. Liew, Mol. Inf. **37**, e1700092 (2017).